Harnessing structure-activity relationship to engineer a cisplatin nanoparticle for enhanced antitumor efficacy

Abhimanyu S. Paraskar[a,b,1], Shivani Soni[a,b,1], Kenneth T. Chin[c], Padmaparna Chaudhuri[a,b], Katherine W. Muto[c], Julia Berkowitz[c], Michael W. Handlogten[d], Nathan J. Alves[d], Basar Bilgicer[d], Daniela M. Dinulescu[b,c], Raghunath A. Mashelkar[e,2], and Shiladitya Sengupta[a,b,c,f,g,h,i,2]

[a]Department of Medicine, Brigham and Women's Hospital, Cambridge, MA 02139; [b]Harvard Medical School, Boston, MA 02115; [c]Department of Pathology, Brigham and Women's Hospital, Boston, MA 02115; [d]University of Notre Dame, Notre Dame, IN 46556; [e]National Chemical Laboratories, Pune 411008, India; [f]Harvard–MIT Division of Health Sciences and Technology, Cambridge, MA 02139; [g]Indo–US Joint Center for Nanobiotechnology, Cambridge, MA 02139; [h]Dana Farber Cancer Institute, Brookline, MA 02445; and [i]Translational Health Science and Technology Institute, New Delhi 110067, India

Contributed by Raghunath A. Mashelkar, May 22, 2010 (sent for review March 2, 2010)

Cisplatin is a first line chemotherapy for most types of cancer. However, its use is dose-limited due to severe nephrotoxicity. Here we report the rational engineering of a novel nanoplatinate inspired by the mechanisms underlying cisplatin bioactivation. We engineered a novel polymer, glucosamine-functionalized polyisobutylene-maleic acid, where platinum (Pt) can be complexed to the monomeric units using a monocarboxylato and an O → Pt coordinate bond. We show that at a unique platinum to polymer ratio, this complex self-assembles into a nanoparticle, which releases cisplatin in a pH-dependent manner. The nanoparticles are rapidly internalized into the endolysosomal compartment of cancer cells, and exhibit an IC50 ($4.25 \pm 0.16\ \mu$M) comparable to that of free cisplatin ($3.87 \pm 0.37\ \mu$M), and superior to carboplatin ($14.75 \pm 0.38\ \mu$M). The nanoparticles exhibited significantly improved antitumor efficacy in terms of tumor growth delay in breast and lung cancers and tumor regression in a K-ras$^{LSL/+}$/Pten$^{fl/fl}$ ovarian cancer model. Furthermore, the nanoparticle treatment resulted in reduced systemic and nephrotoxicity, validated by decreased biodistribution of platinum to the kidney as quantified using inductively coupled plasma spectroscopy. Given the universal need for a better platinate, we anticipate this coupling of nanotechnology and structure-activity relationship to rationally reengineer cisplatin could have a major impact globally in the clinical treatment of cancer.

chemotherapy | nanomedicine | cancer

In the continuing search for effective treatments for cancer, an emerging paradigm is the use of nanotechnology to uncap the full potential of existing chemotherapy agents (1). Integral physicochemical properties of nanovectors can be modulated to improve the antitumor efficacy of chemotherapeutic agents (2). For example, the shape and size of nanostructures can play a deterministic role in the biological outcome (3–5). Similarly, surface modifications to increase hydrophilicity can mask the nanovectors from the reticuloendothelial system, thereby increasing circulation time and altering the pharmacokinetics of the active agents (2). Such nanovectors accumulate preferentially in the tumors due to the unique leaky tumor vasculature coupled with impaired intratumoral lymphatic drainage, which contributes to an enhanced permeation and retention (EPR) effect (6, 7). Indeed, nanovectors were shown to deliver between 5–11× more doxorubicin to Kaposi sarcoma lesions than to normal skin (8). Similarly, the tumor paclitaxel concentration-time area under the curve was found to be 33% higher when administered as an albumin-paclitaxel nanoparticle, and is currently approved for use in metastatic breast cancer (9).

Cisplatin [cis-dichlorodiammineplatinum(II)] is one of the most commonly used chemotherapeutic agents besides doxorubicin and paclitaxel, and is a first line therapy for most malignancies, including testicular, ovarian, cervical, and lung cancer (10). It was also shown recently to be effective in triple negative breast cancer (11). Its clinical use, however, is dose-limited due to systemic toxicity, primarily to the kidney (12). Consequently, developing an improved cisplatin has been a holy grail in cancer drug discovery. We rationalized that this challenge could be addressed by harnessing a nanotechnology-based strategy. It is now well-documented that nanoparticles >5 nm will avoid renal clearance (13), and thereby could potentially reduce cisplatin nephrotoxicity.

The development of a cisplatin nanoparticle has been a challenge resulting from its physicochemical properties, which make it difficult to entrap it in polymeric sustained-release nanoparticles (14, 15). In a recent study, Dhar et al. generated a platinum (IV) complex (*c,t,c*-[$Pt(NH_3)_2(O_2CCH_2CH_2CH_2CH_2CH_3)_2Cl_2$]), which had sufficient hydrophobicity for encapsulation in PLGA-b-PEG nanoparticles, but the prodrug had to be intracellularly processed into cisplatin (16). Alternative strategies based on the conjugation of platinum to polymers (for example, a polyamidoamine dendrimer-platinum complex), resulted in 200–550-fold reduction in cytotoxicity than free cisplatin as a result of strong bonds that are formed between the polymer and Pt (17). Similarly, AP5280, a N-(2-hydroxypropyl) methacrylamide copolymer-bound platinum was found to exert minimal nephrotoxicity in clinical studies (18), but was less potent than carboplatin as the platinum is held to an aminomalonic acid chelating agent coupled to the COOH-terminal glycine of a tetrapeptide spacer (19). These studies also shed light on the impact of the complexation environment of the platinum on the efficacy. We used this structure-activity relationship underlying the activation of platinum to engineer a unique nanoplatinate that exhibited significantly improved antitumor efficacy in terms of tumor growth delay in lung and breast cancer and tumor regression in K-ras$^{LSL/+}$/Pten$^{fl/fl}$ ovarian cancer models, along with reduced systemic and nephrotoxicity.

Results

Cisplatin Bioactivation-Inspired Polymer Design for Nanoparticle Engineering. Cisplatin gets rapidly activated through intracellular

Author contributions: A.S.P., S. Soni, K.T.C., P.C., M.W.H., N.J.A., B.B., D.M.D., R.A.M., and S. Sengupta designed research; A.S.P., S. Soni, K.T.C., P.C., K.W.M., J.B., M.W.H., and N.J.A. performed research; A.S.P., S. Soni, K.T.C., P.C., K.W.M., J.B., M.W.H., N.J.A., B.B., D.M.D., and S. Sengupta analyzed data; and A.S.P., S. Soni, M.W.H., N.J.A., B.B., D.M.D., R.A.M., and S. Sengupta wrote the paper.

The authors declare no conflict of interest.

Freely available online through the PNAS open access option.

[1]A.P. and S.Soni contributed equally to this work.

[2]To whom correspondence may be addressed. Email: ssengupta2@partners.org or ram@ncl.res.in.

This article contains supporting information online at www.pnas.org/lookup/suppl/doi:10.1073/pnas.1007026107/-/DCSupplemental.

aquation of the chloride leaving groups to form *cis*-$[Pt(NH_3)_2Cl(OH_2)]^+$ and *cis*-$[Pt(NH_3)_2(OH_2)]^{2+}$, following which Pt forms covalent bonds to the N7 position of purine bases to form prevalent GpG and ApG intrastrand and interstrand crosslinks (20). In comparison, carboplatin and oxaliplatin have a cyclobutane-1, 1-dicarboxylato and an oxalate respectively as the leaving groups, which chelate the platinum more strongly conferring greater stability to the leaving group-Pt complex (Fig. 1) (21). As a result both carboplatin and oxaliplatin exhibit improved nephrotoxicity profile but also lesser efficacy than cisplatin (22, 23). We rationalized that the design of a nanoparticle modeled on the leaving group would offer the greatest possibility of retaining the efficacy of cisplatin while the size of nanoparticle could bypass renal clearance and thereby reduce nephrotoxicity. As the first step, we identified a polymer, where each monomeric unit could serve as the leaving group of cisplatin. As shown in Fig. 1, hydrolysis of poly-isobutylene-maleic anhydride, comprised of 40 units of maleic acid linked linearly through an isobutylene linker, resulted in the generation of poly-isobutylene-maleic acid (PIMA), where each monomer can be complexed to *cis*-$[Pt(NH_3)_2(OH_2)]^{2+}$ through dicarboxylato linkages. Complexing all 40 monomeric units of the polymer with Pt resulted in gelation. However, lower Pt to polymer ratio resulted in self-assembly into nanoparticles as revealed by dynamic laser light scatter (DLS), with the size being governed by the Pt:polymer unit ratio [Fig. 2*A*]. At a Pt:polymer ratio of 15 : 1, we obtained nanoparticles that were narrowly distributed in 80–140 nm size range. It is now well-established that nanoparticles in the optimal size range of 80–160 nm home preferentially into tumors resulting from the EPR effect (7), suggesting that the polymeric-cisplatin nanoparticle (PIMA-cisplatin) could potentially reduce systemic side effects and exhibit increased intratumoral delivery. We next tested the PIMA-cisplatin nanoparticle on a Lewis lung carcinoma cell line in vitro. As shown in Fig. 3*A* whereas PIMA-cisplatin nanoparticle induced cell kill, the efficacy was significantly lower than free cisplatin and similar to carboplatin, consistent with the stable dicarboxylato complexation between the platinum and the maleic acid monomers (22, 23).

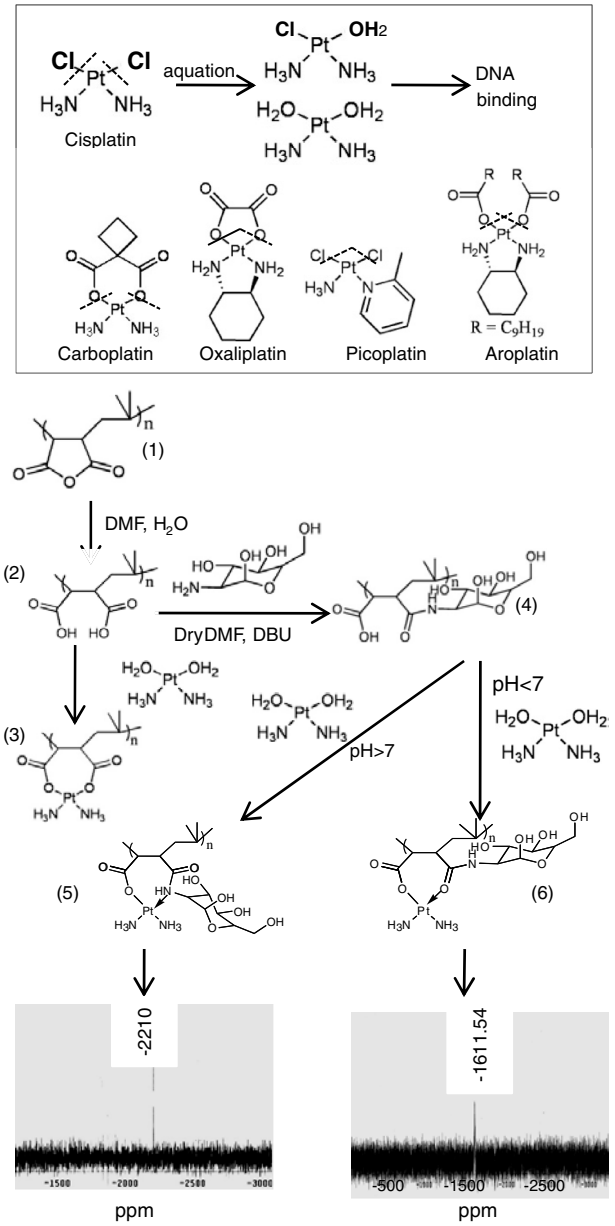

Fig. 1. Structure-activity relationship inspired engineering of a cisplatin nanoparticle. (*A*) Schematic shows the mechanism underlying the intracellular activation of cisplatin and analogues through aquation (dash lines). (*B*) Scheme shows the synthesis of PIMA-cisplatin and PIMA-glucosamine (PIMA-GA)-cisplatin complex. Transformation of polymaleic anhydride ($n = 40$) (*1*) to polymaleic acid [PIMA] (*2*) enables complexation of $[NH_2]_2Pt[OH]_2$ through dicarboxylato bonds (*3*). Derivatization of one arm of PIMA with glucosamine to generate PIMA-GA (*4*), and complexation with $[NH_2]_2Pt[OH]_2$ can lead to two isomers (*5*, *6*) depending on pH, characterized by unique NMR signatures.

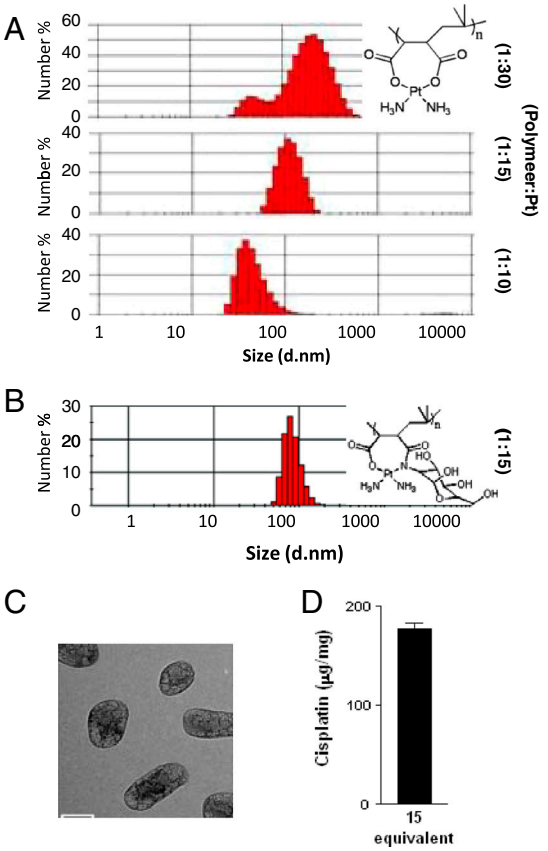

Fig. 2. Physicochemical characterization of nanoparticles. (*A*). Graphs show the relationship between the size distribution of PIMA-cisplatin nanoparticles as a function of polymer to platinum ratio as measured by DLS. (*B*) Size distribution of PIMA-GA-CisPt (O → Pt) nanoparticle at a 15 : 1 Pt : polymer ratio measured using DLS. (*C*) Representative high-resolution TEM images of PIMA-GA-cisplatin nanoparticles Bar = 125 nm (*D*) Graph shows the total platinum loaded per mg of polymer at this ratio. The data shown are mean ± SE from $n =$ at least 3 independent experiments.

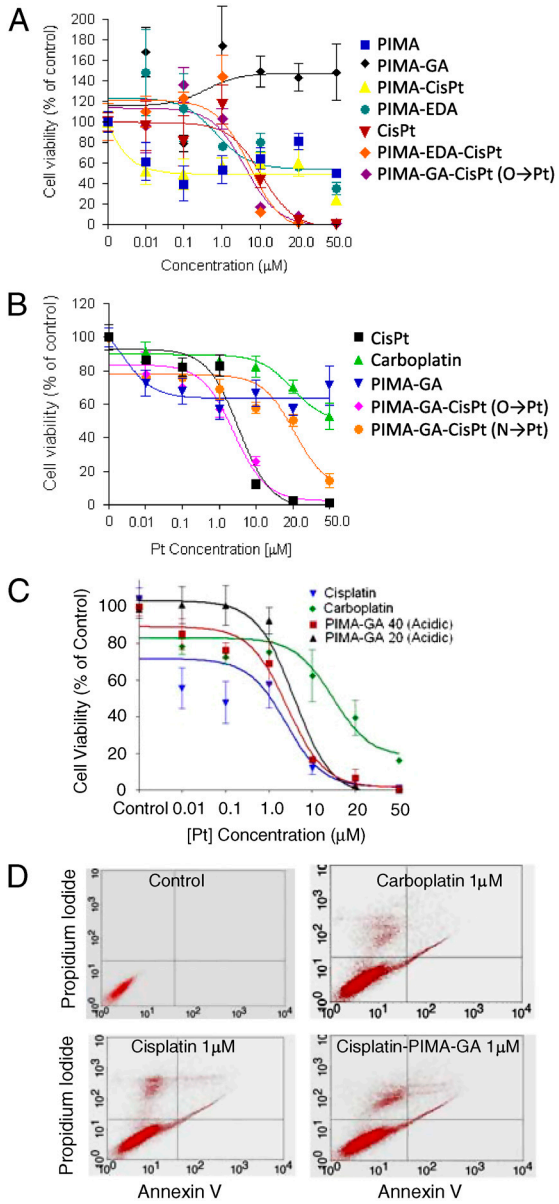

Fig. 3. In vitro characterization of cisplatin nanoparticle. Graphs show the concentration-effect of different treatments on cellular viability of (*A*) LLC and (*B*) 4T1 breast cancer cells as measured using MTS assay. The x-axis shows the equivalent concentrations of platinum. Where blank polymeric controls were used, dose of polymer used was equivalent to that used to deliver that specific dose of cisplatin in the complexed form. (*C*) Graph shows effect of PIMA-GA-cisplatin (O → Pt) nanoparticles on LLC cells viability, where the either 20 or all 40 monomers of the PIMA backbone is derivatized with glucosamine, thereby altering the Pt environment. (*D*) Representative FACS images of LLC cells labeled with Annexin V-FITC and PI to monitor apoptosis and necrosis. Cells were incubated with the drugs for 24 h. The data shown are mean ± SE, $n = 3$.

Rational Optimization of the Polymer Based on Structure-Activity Relationship. As the next step, to improve efficacy of the nanoparticles, we rationalized that derivatizing one arm of each monomer unit of the polymer with biocompatible glucosamine to generate a PIMA-glucosamine conjugate (PIMA-GA) would convert the dicarboxylato bonds with Pt to a monocarboxylato bond and a coordinate bond, which should release Pt more easily (Fig. 1). NMR characterization of the Pt environment revealed that complexation of PIMA-GA and cisplatin in an acidic pH generated an isomeric molecule, [PIMA-GA-cisplatin (O → Pt)], characterized by the monocarboxylato and a O → Pt coordination complex as indicated by a single Pt NMR peak at −1611.54 ppm. Complexing the cisplatin with PIMA-GA at an alkaline pH (pH 8.5) favored the formation of an isomeric PIMA-GA-cisplatin (N → Pt) complex, where the Pt is complexed through a monocarboxylato and a more stable N → Pt coordinate bond characterized by a unique peak at −2210 ppm. The possibility of generating these two pH-dependent states allowed us to further dissect the impact of Pt environment, specifically the leaving groups, on the biological efficacy. The complexation of cisplatin to PIMA-glucosamine (PIMA-GA) polymer at a ratio of 15:1 resulted in self-assembly into nanoparticles in the desired narrow size bandwidth of 80–150 nm as confirmed by DLS (Fig. 2*B*) and high-resolution transmission electron microscopy (TEM) (Fig. 2*C*). Furthermore, we achieved a loading of 175 ± 5 μg/mg of polymer (Fig. 2*D*), which is significantly higher than can be achieved using traditional nanoparticle formulations (14, 15).

Characterizing the Uptake and Efficacy of Nanoparticles In Vitro. To test the efficacy of the PIMA-GA-cisplatin nanoparticles in vitro, we performed cell viability assays using Lewis lung carcinoma (LLC) and 4T1 breast cancer cell lines. Cell viability was quantified using a 3-(4,5-dimethylthiazol-2-yl)-5-(3-carboxymethoxyphenyl)-2-(4-sulfophenyl)-2H-tetrazolium, inner salt (MTS) assay at 48 h postincubation. The LLC cells (Fig. 3*A*) were more susceptible to the cisplatin-nanoparticles than the 4T1 breast cancer cells (Fig. 3*B*). PIMA-GA-cisplatin (O → Pt) nanoparticles demonstrated significant LLC cell kill (IC50 = 4.25 ± 0.16 μM) comparable to cisplatin (IC50 = 3.87 ± 0.37 μM) and superior to carboplatin (IC50 = 14.75 ± 0.38 μM), supporting the hypothesis that the rate of aquation is critical for efficacy (Fig. 3). A similar efficacy was observed when we replaced glucosamine with ethylene diamine, which creates a similar Pt complexation environment as glucosamine (Fig. 3*A*). This was additionally supported by the observation that PIMA-GA-cisplatin (N → Pt) nanoparticles (IC50 = 6.36 ± 0.19 μM) were significantly less active than cisplatin, suggesting that the platinum environment is critical in defining the rate of aquation. To further validate the role of complexation environment, we generated PIMA-GA (20), where only 20 of the 40 monomers comprising a PIMA polymer were derivatized with glucosamine, thereby introducing a mixture of dicarboxylato bonds and monocarboxylato plus coordinate bonds that complex Pt to PIMA-GA. As shown in Fig. 3*C*, the concentration-efficacy curve shifts to the right with PIMA-GA(20)-cisplatin (IC50 = 5.85 ± 0.13 μM) as compared with PIMA-GA-cisplatin (O → Pt) nanoparticles, where all the 40 monomers are derivatized with glucosamine. Empty PIMA-GA polymer had no effect on the cell viability.

Labeling the cells for expression of phosphatidylserine on the cell surface revealed that the cisplatin nanoparticle treatment could induce apoptotic cell death, with LLCs being more susceptible than 4T1 cells (Fig. 3*D* and Fig. S1). Tagging the polymer with fluorescein (Fig. S2) enabled the temporal tracking of uptake of the nanoparticles into the cells, which were colabeled with a lysotracker-red dye to label the endolysosomal compartments. As shown in Fig. S2, a rapid uptake of the nanoparticles and internalization into the endolysosomal compartment was observed in the LLC cells within 15 min of treatment with in contrast to 2 h in the case of 4T1 cells.

Release of Active Cisplatin from Nanoparticle Is pH-Dependent. As the nanoparticles localized to the lysosomal compartment, we tested the release of Pt from the nanoparticles at pH 5.5, mimicking the acidic pH of the endolysosomal compartment of the tumor (24). We also selected pH 8.5 as a reference pH in the alkaline range. As shown in Fig. 4, at pH 5.5 PIMA-GA-cisplatin (O → Pt) nanoparticles resulted in a sustained release of cisplatin monitored over a 70 h period. In contrast the release at pH 8.5 was significantly lower, indicating a pH-dependent release of Pt. PIMA-

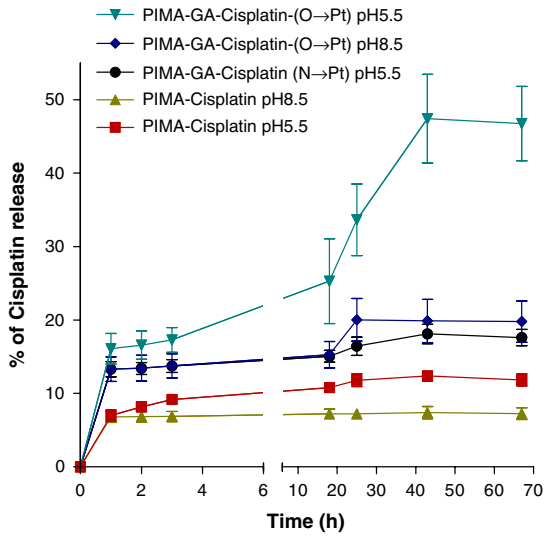

Fig. 4. Graph shows the pH-dependent release of cisplatin from the nanoparticles. The nanoparticles were incubated at pH 5.5 or pH 8.5 in a dialysis bag, and release over time was quantified. The data shown are mean ± SE from $n = 3$.

GA-cisplatin (N → Pt) released Pt at a slower rate even at pH 5.5, consistent with the fact that the N → Pt coordinate bond is stronger than the O → Pt linkage. As expected, we observed that PIMA-cisplatin nanoparticles exhibited significantly lower rates of Pt release as compared with both PIMA-GA-cisplatin (N → Pt) and PIMA-GA-cisplatin (O → Pt) as the Pt is held by more stable dicarboxylato bonds instead of a monocarboxylato and a coordinate bond.

Nanoparticle Induces Tumor Growth Delay and Regression with Reduced Nephrotoxicity. As PIMA-GA-cisplatin (O → Pt) nanoparticles exhibited the desired release rates for platinum and also exhibited in vitro efficacy comparable to cisplatin, we validated the therapeutic efficacy of these nanoparticles in vivo. Mice bearing established 4T1 breast cancer were randomized into five groups and treated thrice with (*i*) vehicle (PBS) control; (*ii*) Cisplatin (1.25 mg/kg); (*iii*) Cisplatin (3 mg/kg); (*iv*) PIMA-GA-Cisplatin (O → Pt) nanoparticles (1.25 mg/kg); and (*v*) PIMA-GA-Cisplatin (O → Pt) nanoparticles (3 mg/kg). The mice injected with vehicle formed large tumors by day 16 and were euthanized. The animals in the other groups were also sacrificed at the same time point to evaluate the effect of the treatments on tumor pathology. As shown in Fig. 5, whereas both free cisplatin and the cisplatin-nanoparticles exhibited similar tumor inhibition, the free drug resulted in a significant reduction in body weight indicating systemic toxicity. Furthermore, necropsy revealed that treatment with free cisplatin results in a significant reduction in the weights of kidney and spleen, indicating nephrotoxicity and hematotoxicity consistent with previous reports. In contrast, cisplatin nanoparticles had no effect on the weights of the kidneys or the spleen (Fig. 5 *D* and *E*). To elucidate the mechanism underlying cytotoxicity, we TUNEL-stained tumor sections, which revealed a significant induction of apoptosis following treatment with both free cisplatin and PIMA-GA-cisplatin (O → Pt) nanoparticles (Fig. 5*F*). Labeling the kidney sections for TUNEL validated significant apoptosis in the animals treated with free cisplatin as opposed to minimal nephrotoxicity in the nanoparticle-treated group (Fig. 5*F*). Indeed, biodistribution studies using inductively coupled plasma-spectrometry revealed that the concentration of Pt in the kidney following administration of the cisplatin-nanoparticle is negligible as compared to that attained following administration of free drug (Fig. 5*G*), which can explain the reduction in nephrotoxicity. Similarly, the concentration of platinum in the reticuloendothelial system (RES) was lower when administered as a nanoparticle as compared with free cisplatin or carboplatin, indicating that the nanoparticles can escape the RES. In a separate experiment, animals bearing Lewis lung carcinoma were similarly treated and exhibited similar superior outcome with the nanoparticles (Fig. S3).

We next evaluated the PIMA-GA-cisplatin (O → Pt) nanoparticles in a K-ras$^{LSL/+}$/Pten$^{fl/fl}$ ovarian cancer model, in which cisplatin is a first line drug of choice. The discovery of frequent somatic *PTEN* mutations and loss of heterozygosity at the 10q23 *PTEN* locus in endometrioid ovarian cancer implicates a key role for *PTEN* in the etiology of this epithelial ovarian cancer subtype (25, 26). Similarly, *K-RAS* oncogene is also mutated in endometrioid ovarian cancer, albeit at a lesser frequency (27). In a recent study, the combination of these two mutations in the ovarian surface epithelium was found to induce invasive and widely metastatic endometrioid ovarian adenocarcinomas with complete penetrance, making it a good model for mimicking

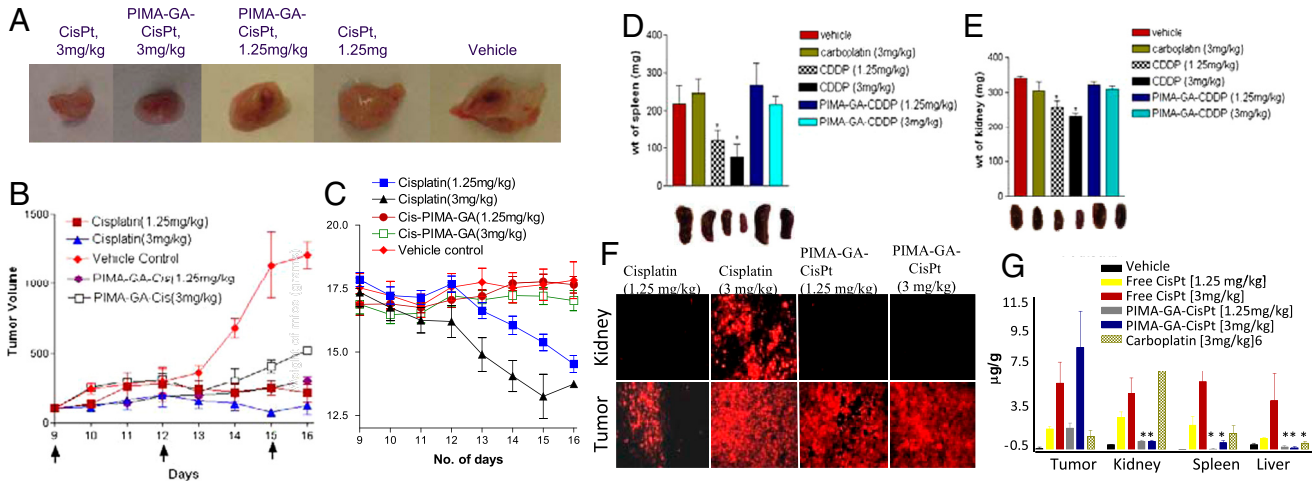

Fig. 5. In vivo characterization of PIMA-GA-cisPt nanoparticle in a 4T1 breast cancer model. (*A*) Representative 4T1 breast tumors excised from animals treated with cisplatin or PIMA-GA-cisPt (O → Pt) nanoparticle. Graphs show the effect of treatments on (*B*) tumor volume, (*C*) body weight, (*D*) spleen weight, and (*E*) kidney weight. The animals were dosed thrice (shown by arrows on x-axis). Data shown are mean ± SE, $n = 4$–8. The images on below of each graph show representative organs from each treatment group. (*F*) Representative images of cross-sections of tumor and kidney stained for TUNEL. Images were captured using a Nikon Ti epifluorescence microscope at low magnification to capture a large view field. (*G*) Tissue distribution of platinum following treatment in free (as cisplatin or carboplatin) or nanoparticle form. ($n = 3$–5 per treatment group.) *$P < 0.05$ vs. vehicle-treated group (ANOVA followed by Newman Keuls Post Hoc test).

human tumor progression (28). Vehicle-treated animals exhibited rapid tumor progression as quantified by luciferase expression. Treatment with the cisplatin-nanoparticles resulted in a dose-dependent inhibition of tumor progression, with the lower dose equivalent to 1.25 mg/kg exerting a similar inhibition as a 3 mg/kg dose of free cisplatin (Fig. 6). Treatment with the higher dose of cisplatin-nanoparticle (equivalent to 3 mg/kg of cisplatin) resulted in greater tumor inhibition without any significant loss of body weight or nephrotoxicity (Fig. 6*D*) compared with equi-dose of free cisplatin. Interestingly, we observed different levels of systemic toxicity in the different mouse strains, indicating distinct levels of susceptibility to the cytotoxic. This can potentially be explained by an enhanced distribution to the tumor with reduced clearance by the RES (Fig. 6*E*).

Discussion

Despite the development of targeted therapeutics (29), cytotoxic chemotherapeutics are still the first line therapy for all tumors. This necessitates novel strategies that can increase the therapeutic index of cytotoxics. In this study, we merged the mechanism of cisplatin bioactivation with the inherent advantages of nanotechnology to rationally engineer a unique polymeric nanoparticle that increases the therapeutic index of cisplatin. Furthermore, we used this platform to validate that the complexation environment of platinum plays a critical role in the efficacy of platinum-based cytotoxics.

Cisplatin is one of the most commonly used cytotoxic agents in cancer chemotherapy, and exerts its activity by interfering with transcription and other DNA-mediated cellular functions (30). In an elegant study, Davies et al. used a 1H-13N heteronuclear sequential quantum correlation NMR spectroscopy to demonstrate that aquation of cisplatin results in the rapid formation of *cis*-$[Pt(NH_3)_2Cl(OH_2)]^+$ and *cis*-$[Pt(NH_3)_2(OH_2)]^{2+}$ (31) with a rate constant of 8×10^{-5} s^{-1}. In contrast the rate constant for aquation of carboplatin was found to be 7.2×10^{-7} s^{-1}. This difference in their rate of activation was matched by their rates of binding to DNA (21, 22), which can explain the increased IC50 value of carboplatin compared with cisplatin (22). This was further validated in our studies as the PIMA-cisplatin nanoparticles, where both the dicarboxylato and the monocarboxylato plus N → Pt linkages confer greater stability to the Pt-polymer complex as seen in the release kinetics experiments. In contrast, we demonstrate that the rational introduction of an O → Pt coordinate linkage facilitates rapid activation of platinum, which can explain the increased efficacy of the PIMA-GA-Cisplatin (O → Pt) nanoparticles. The EPR effect combined with the approximately 100 nm nanoparticle size that exceed the 5 nm cutoff for clearance by the kidney could potentially explain the preferential accumulation of the PIMA-GA-Cisplatin (O → Pt) nanoparticles in the tumor with decreased renal platinum concentration as observed in this study. Together with the rapid release of platinum, this can explain the increased antitumor efficacy of PIMA-GA-Cisplatin (O → Pt) nanoparticle compared with free cisplatin at lower concentrations and increased therapeutic index at the highest concentrations as seen in vivo.

In conclusion, we demonstrate that the rational engineering of a polymer inspired by the bioactivation of cisplatin enables the engineering of a unique nanoplatinate, which improves antitumor efficacy of cisplatin by capitalizing on the inherent properties of nanoscale. This opens up the possibility to increase the maximal tolerated dose of cisplatin, which is an effective chemotherapeutic agent but dose limited due to nephrotoxicity. The clinical familiarity of using an established and globally used chemotherapeutic, together with the low cost of the basic building blocks used in fabricating the nanoparticle, can facilitate the rapid translation of this technology, thereby validating the potential of nanotechnology to impact global health (32).

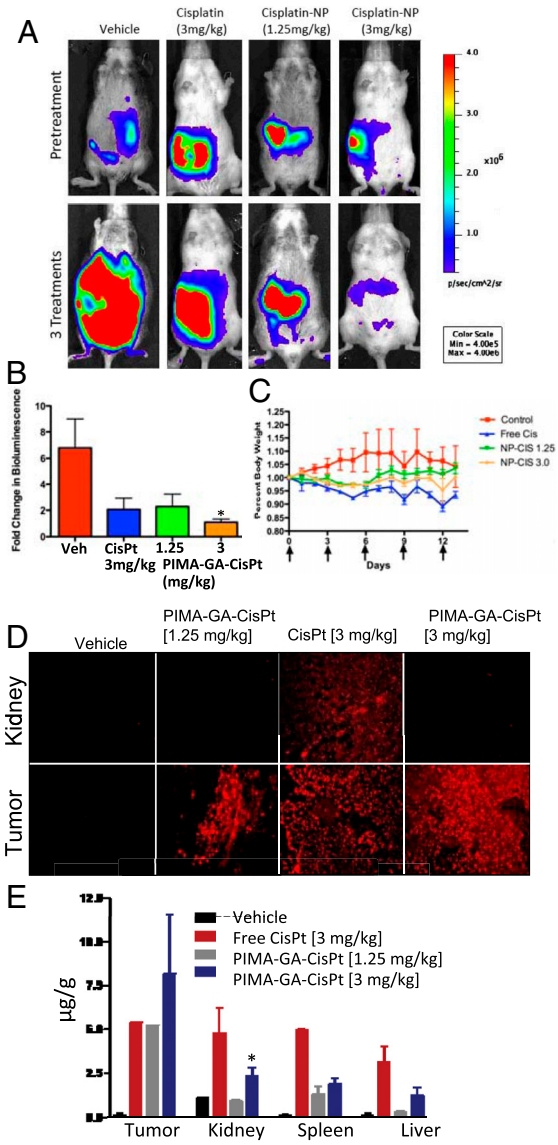

Fig. 6. PIMA-GA-cisplatin nanoparticle inhibits tumor growth in a K-ras$^{LSL/+}$/Pten$^{fl/fl}$ ovarian cancer model. (*A*). Representative pictures from 4 treatment groups before and after treatment. Tumor images was obtained with the IVIS Lumina II Imaging System. Quantification of bioluminescence was achieved by using the Living Image Software 3.1. Mice received 150 mg/kg of D-luciferin firefly potassium salt via intraperitoneal injection prior to imaging. (*B*). Bioluminescence quantification indicates a significantly decreased tumor luciferase signal in mice treated with cisplatin-NP compared to vehicle ($p < 0.05$, one-way ANOVA analysis). (*C*). Graph shows drug toxicity assessed by measurements in overall body weight. Daily recording of body weights indicated a significant loss of body weight in the free cisplatin group as compared to both cisplatin-NP (1.25 mg/kg and 3 mg/kg) treated groups ($p < 0.05$, two-way ANOVA analysis). (*D*) Epifluorescence images of cross sections of tumor treated with free of nanoparticle cisplatin that were stained for TUNEL as a marker for apoptosis. (*E*) Tissue distribution of platinum following treatment in free (as cisplatin or carboplatin) or nanoparticle form. ($n = 3$ per treatment group.) *$P < 0.05$ vs. vehicle-treated group (ANOVA followed by Newman Keuls Post Hoc test).

Materials and Methods

Synthesis of Cisplatin Nanoparticles. Poly(isobutylene-*alt*-maleic anhydride) was dissolved in dry dimethylformamide (DMF) in round bottom flask to which double distilled water was added. Solvent was removed under vacuum and low molecular weight impurities were removed using dialysis (MWCO: 1000 KD, Spectrapor). The solution was then lyophilized to get poly(isobutylene-*alt*-maleic acid) (PIMA). To generate PIMA-glucosamine polymer, poly(isobutylene-*alt*-maleic anhydride) was dissolved in DMF to which

Diaza(1, 3)bicyclo[5.4.0]undecane (DBU) and glucosamine was added. The resulting reaction mixture was allowed to stir at room temperature for 48 h and then quenched by adding double distilled water. The organic solvent was evaporated under vacuum. The resulting pale yellow solid was purified by dialysis. Nanoparticles were engineered by dissolving the polymers in double distilled water containing cisplatin for 48 h. The polymer-cisplatin conjugates were purified by dialysis. The dialyzed solutions were lyophilized, and resuspended to obtain the nanoparticles. The products were characterized at each step using ^{1}H, ^{13}C, and Pt NMR.

Particle Size Measurement. See *SI Text*.

Physicochemical Release Kinetics Studies. See *SI Text*.

In Vitro Cell Viability Assay. See *SI Text*.

FACS Analysis for Apoptosis. See *SI Text*.

Cellular Uptake Studies. See *SI Text*.

In Vivo Murine Lewis Lung Carcinoma and 4T1 Breast Cancer Models. The LLC cells and 4T1 Breast cancer cells (3×10^5) were implanted subcutaneously in the flanks of 4-week-old C57/BL6 and BALB/c mice (weighing 20 g, Charles River Laboratories) respectively. The drug therapy was started on day 6 for LLC and day 9 for the 4T1 tumors. Free or nanoparticle cisplatin was administered through tail vein at doses equivalent to 1.25 and 3 mg/kg of platinum in PBS (100 μL). The tumor volumes, calculated using formula $L \times B^2$, and body weights were monitored on a daily basis. The animals were sacrificed when the average tumor size of the control exceeded 2000 mm^3 in the control group. The tumors were harvested immediately following sacrifice and stored in 10% formalin for further analysis. All animal procedures were approved by the Harvard Institutional Use and Care of Animals Committee.

In Vivo Murine Ovarian Cancer Tumor Model. Ovarian adenocarcinomas were induced in genetically engineered K-$ras^{LSL/+}$/$Pten^{fl/fl}$ mice via intrabursal delivery of adenovirus carrying Cre recombinase, as described previously (28). Tumor cells were engineered to express luciferase once activated by Adeno-Cre, to make tumor imaging feasible before and after drug treatment. Once mice developed medium to large tumors they were placed into one of four treatment groups (tumor imaging in vivo was performed with the IVIS Lumina II Imaging System). Quantification of bioluminescence was achieved by using the Living Image Software 3.1 (Caliper Life Sciences). Mice received 150 mg/kg of D-luciferin firefly potassium salt via i.p. injection prior to imaging. Five min postluciferin injection, animals were anesthetized in a 2.5% isoflurane induction chamber. Once anesthesized, mice were placed into the imaging chamber where they were kept under anesthesia by a manifold supplying isoflurane and their body temperature was maintained by a 37 °C temperature stage. Bioluminescent signal was collected 15 min after luciferin administration for an exposure time of 30 s. Images were taken a day prior to treatment (day 0, baseline) and 1 d following the final treatment. Treatment efficacy was quantified by examining the fold increase in bioluminescence of the posttreatment signal as compared to baseline.

Biodistribution of Cisplatin. See *SI Text*.

Histopathology and TUNEL Assay (Apoptotic Assay). See *SI Text*.

Toxicity Assessment of Drug Treatment. Body weights were recorded daily to assess toxicity. In addition, livers and spleens were removed at the end of treatment to record weights and perform extensive pathological examination to assess toxicity of vital organs. Cell apoptosis in vital organs was measured using TUNEL assay.

Statistical Analysis. Data were expressed as means ± S.D from at least $n = 3$. Statistical analysis was conducted using the Prism software (GraphPad). The statistical differences were determined by ANOVA followed by Newman Keuls Post Hoc test or Student's t test. $p < 0.05$ was considered to indicate significant differences.

ACKNOWLEDGMENTS. S. Sengupta is supported by US Department of Defense (DOD) Breast Cancer Research Program (BCRP) Era of Hope Scholar Award W81XWH-07-1-0482, a DOD Collaborative Innovator Grant, and National Institutes of Health Grant R01 (1R01CA135242-01A2). A.P. is supported by a DOD BCRP postdoctoral fellowship award. D.M.D. is supported by the Burroughs-Wellcome Foundation, a Harvard Ovarian Cancer Spore Award, the Canary Fund, the Mary Kay Ash Foundation, and the V Foundation for Cancer Research Scholar award.

1. Ferrari M (2005) Cancer nanotechnology: Opportunities and challenges. *Nat Rev Cancer* 5:161–171.
2. Moghimi SM, et al. (2001) Long-circulating and target-specific nanoparticles: Theory to practice. *Pharmacol Rev* 53:283–318.
3. Decuzzi P, et al. (2009) Intravascular delivery of particulate systems: Does geometry really matter? *Pharm Res* 26:235–243.
4. Chaudhuri P, et al. (2010) Shape effect of carbon nanovectors on angiogenesis. *ACS Nano* 4:574–582.
5. Gratton SE, et al. (2008) The effect of particle design on cellular internalization pathways. *Proc Natl Acad Sci USA* 105:11613–11618.
6. Yuan F, et al. (1995) Vascular permeability in a human tumor xenograft: Molecular size dependence and cutoff size. *Cancer Res* 55:3752–3756.
7. Yuan F, et al. (1994) Microvascular permeability and interstitial penetration of sterically stabilized (stealth) liposomes in a human tumor xenograft. *Cancer Res* 54:3352–3356.
8. Northfelt DW, et al. (1996) Doxorubicin encapsulated in liposomes containing surface-bound polyethylene glycol: Pharmacokinetics, tumor localization, and safety in patients with AIDS-related Kaposi's sarcoma. *J Clin Pharmacol* 36:55–63.
9. Desai N, et al. (2006) Increased antitumor activity, intratumor paclitaxel concentrations, and endothelial cell transport of cremophor-free, albumin-bound paclitaxel, ABI-007, compared with cremophor-based paclitaxel. *Clin Cancer Res* 12:1317–1324.
10. Kelland L (2007) The resurgence of platinum-based cancer chemotherapy. *Nat Rev Cancer* 7:573–584.
11. Leong CO, et al. (2007) The p63/p73 network mediates chemosensitivity to cisplatin in a biologically defined subset of primary breast cancers. *J Clin Invest* 117:1370–1380.
12. Madias NE, Harrington JT (1978) Platinum nephrotoxicity. *Am J Med* 65:307–314.
13. Choi HS, et al. (2007) Renal clearance of quantum dots. *Nat Biotechnol* 25:1165–1170.
14. Avgoustakis K, et al. (2002) *PLGA*-mPEG nanoparticles of cisplatin: In vitro nanoparticle degradation, in vitro drug release, and in vivo drug residence in blood properties. *J Controlled Release* 79:123–135.
15. Fujiyama J, et al. (2003) Cisplatin incorporated in microspheres: Development and fundamental studies for its clinical application. *J Controlled Release* 89:397–408.
16. Dhar S, et al. (2008) Targeted delivery of cisplatin to prostate cancer cells by aptamer functionalized Pt(IV) prodrug-PLGA-PEG nanoparticles. *Proc Natl Acad Sci USA* 105:17356–17361.
17. Haxton KJ, Burt MH (2009) Polymeric drug delivery of platinum-based anticancer agents. *J Pharm Sci* 98:2299–2316.
18. Rademaker-Lakhai JM, et al. (2004) A Phase I and pharmacological study of the platinum polymer AP5280 given as an intravenous infusion once every 3 weeks in patients with solid tumors. *Clin Cancer Res* 10:3386–3395.
19. Lin X, et al. (2004) Improved targeting of platinum chemotherapeutics. The antitumour activity of the HPMA copolymer platinum agent AP5280 in murine tumour models. *Eur J Cancer* 40:291–297.
20. Huang H, et al. (1995) Solution structure of a cisplatin-induced DNA interstrand cross-link. *Science* 270:1842–1845.
21. Hongo A, et al. (1994) A comparison of in vitro platinum-DNA adduct formation between carboplatin and cisplatin. *Int J Biochem* 26:1009–1016.
22. Knox RJ, et al. (1986) Mechanism of cytotoxicity of anticancer platinum drugs: Evidence that *cis*-diamminedichloroplatinum(II) and *cis*-diammine-(1,1-cyclobutanedicarboxylato)platinum(II) differ only in the kinetics of their interaction with DNA. *Cancer Res* 46:1972–1979.
23. Go RS, et al. (1999) Review of the comparative pharmacology and clinical activity of cisplatin and carboplatin. *J Clin Oncol* 17:409–422.
24. Song CW, et al. (2006) Influence of tumor pH on therapeutic response. *Cancer Drug Discovery and Development: Cancer Drug Resistance*, ed B Teicher (Humana Press, Totowa, NJ), pp 21–42.
25. Obata K, et al. (1998) Frequent PTEN/MMAC1 mutations in endometrioid but not serous or mucinous epithelial ovarian tumors. *Cancer Res* 58:2095–2097.
26. Sato N, et al. (2000) Loss of heterozygosity on 10q23.3 and mutation of the tumor suppressor gene *PTEN* in benign endometrial cyst of the ovary: Possible sequence progression from benign endometrial cyst to endometrioid carcinoma and clear cell carcinoma of the ovary. *Cancer Res* 60:7052–7056.
27. Cuatrecasas M (1998) K-ras mutations in nonmucinous ovarian epithelial tumors. *Cancer* 82:1088–1095.
28. Dinulescu DM (2005) Role of K-ras and Pten in the development of mouse models of endometriosis and endometrioid ovarian cancer. *Nat Med* 11:63–70.
29. Shawver LK, et al. (2002) Smart drugs: Tyrosine kinase inhibitors in cancer therapy. *Cancer Cell* 1:117–123.
30. Jamieson ER, Lippard SJ (1999) Structure, recognition, and processing of cisplatin-DNA adducts. *Chem Rev* 99:2467–2498.
31. Davies MS, et al. (2000) Slowing of cisplatin aquation in the presence of DNA nut not in the presence of phosphate. Improved understanding of the sequence selectivity and the roles of monoaquated and diaquated species in the binding of cisplatin to DNA. *Inorg Chem* 39:5603–5613.
32. Salamanca-Buentello F, et al. (2005) Nanotechnology and the developing world. *PLoS Med* 2:e97.